Supporting information

Tris(ethylenediamine) cobalt(II) and manganese(II) nitrates

Miguel Cortijo, Ángela Valentín-Pérez, Mathieu Rouzières, Rodolphe Clérac, Patrick Rosa and Elizabeth A. Hillard

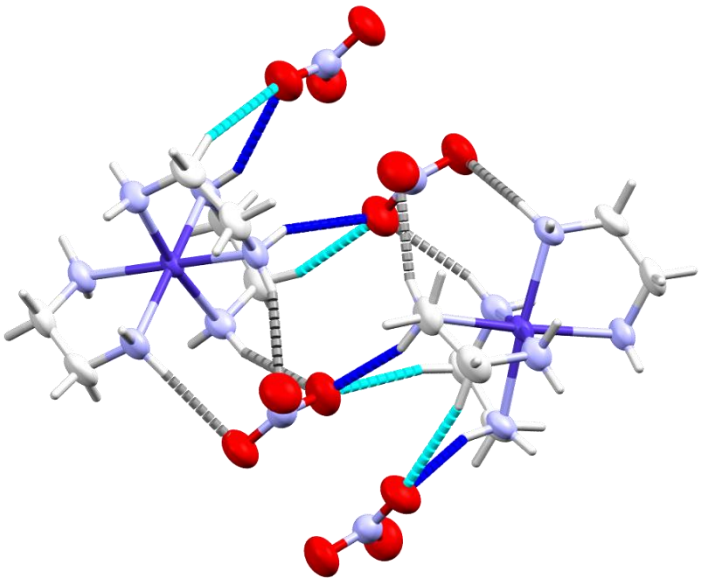

Figure S1. Cation-anion close contacts shown in Λ-[Co(en)$_3$](NO$_3$)$_2$ at 298 K. Contact color code: Gray = 2.327 Å, dark blue = 2.426 and light blue = 2.517 Å.

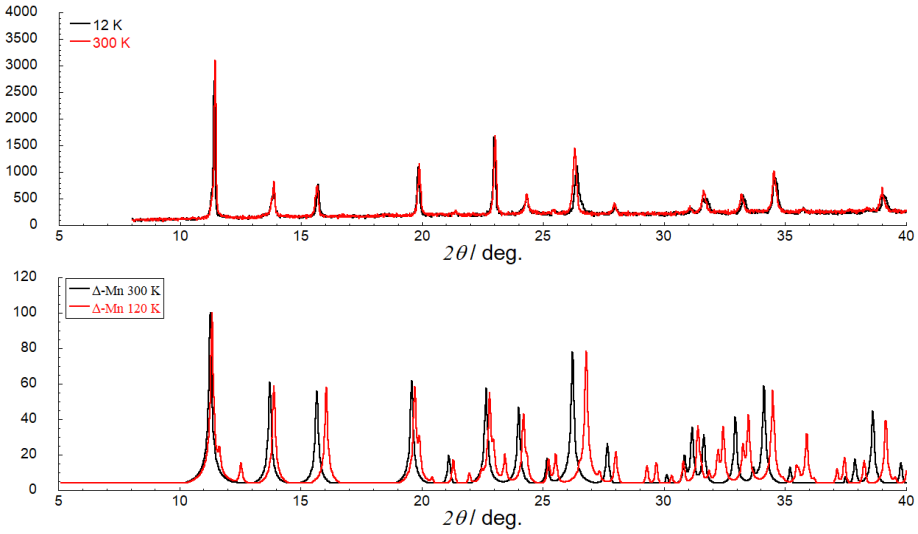

Figure S2. (top) Powder X-ray diffractograms for [Co(en)$_3$](NO$_3$)$_2$ at 12 and 300 K showing no change with temperature; (bottom) Powder diffractograms simulated from Δ-[Mn(en)$_3$](NO$_3$)$_2$ single crystal data at 120 and 300 K, which demonstrate the expected change upon the phase transition.

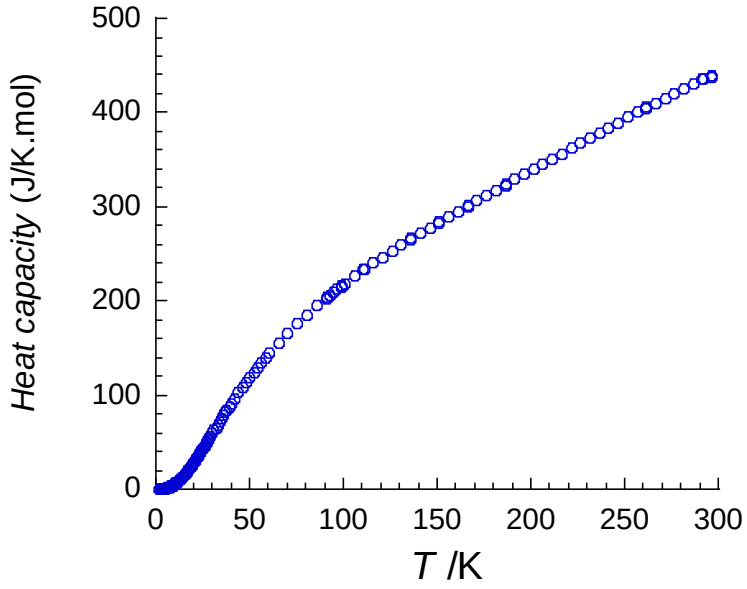

Figure S3. Heat capacity trace for a polycrystalline sample of $[Co(en)_3](NO_3)_2$. The featureless curve is taken as evidence for the lack of phase transition down to 2 K.

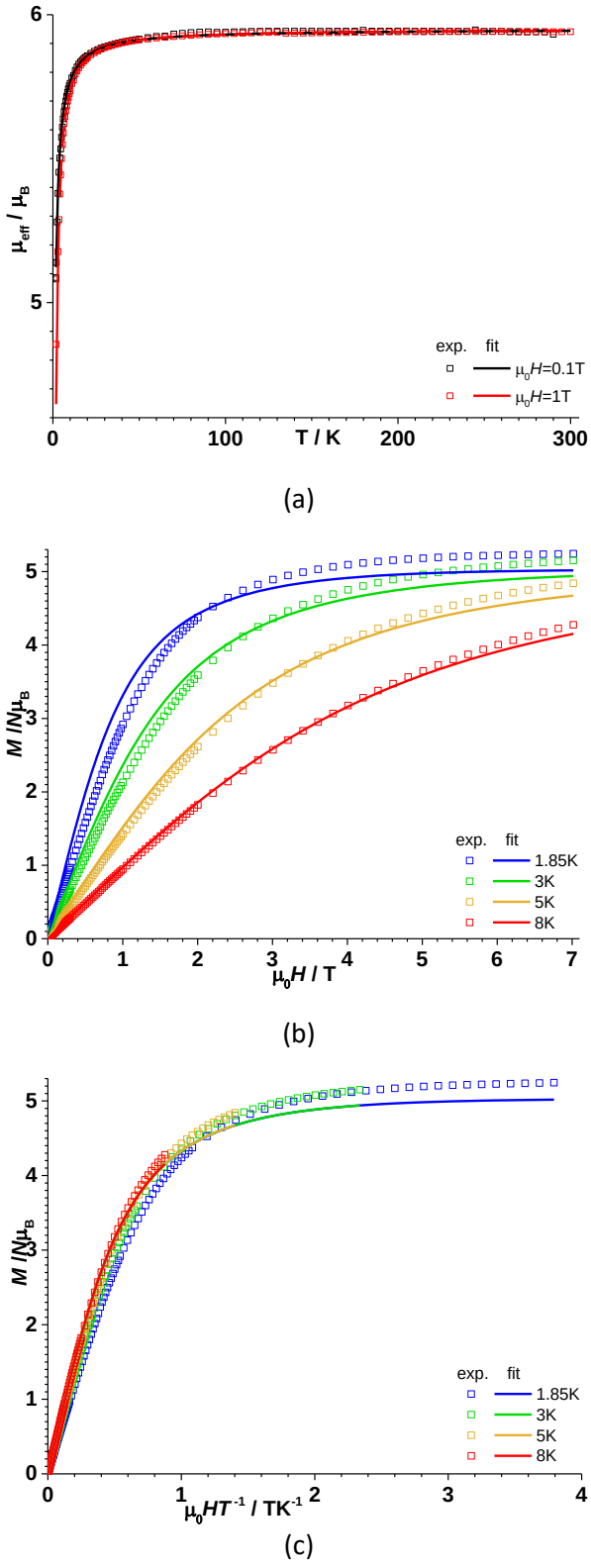

Figure S4. Magnetic behavior of $[Mn(en)_3](NO_3)_2$. (a) μ_{eff} vs. T plot for magnetic fields of 0.1 (experimental points as black squares, and fit as black dotted line) and 1 T (experimental points as red squares, and fit as red dotted line); (b) isothermal M vs. H plot (squares) and corresponding fit (lines) for 1.85 (blue), 3 (green), 5 (yellow) and 8 K (red); (c) isothermal M vs. H/T plot (squares) and corresponding fit (lines) for 1.85 (blue), 3 (green), 5 (yellow) and 8 K (red).

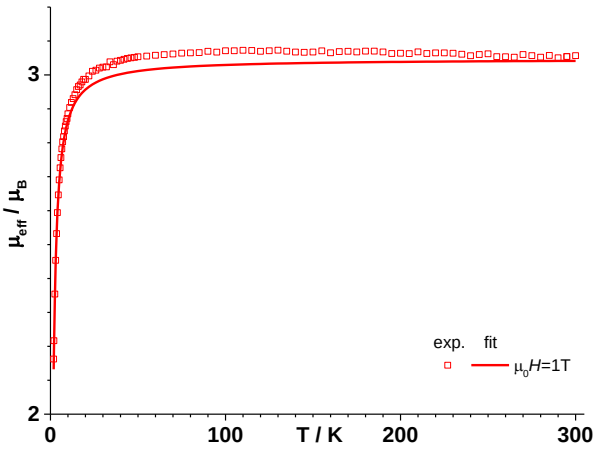

(a)

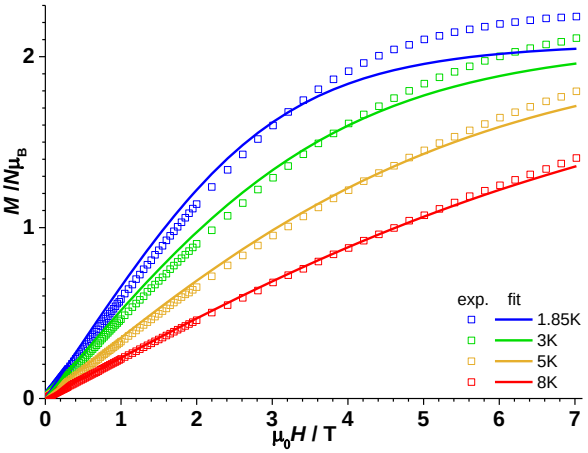

(b)

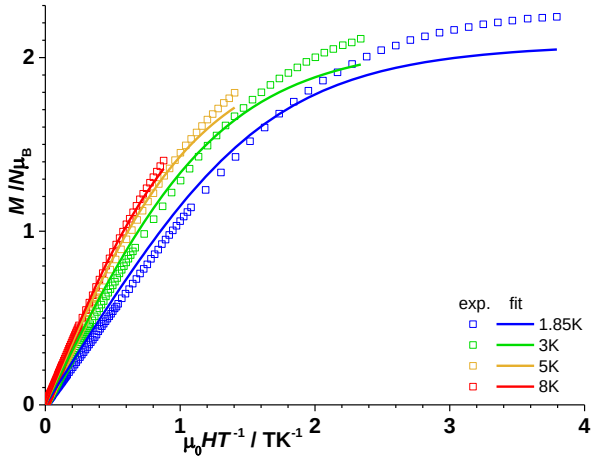

(c)

Figure S5. Magnetic behavior of $[Ni(en)_3](NO_3)_2$. (a) μ_{eff} vs. T plot for magnetic fields of 0.1 (experimental points as black squares, and fit as black dotted line) and 1 T (experimental points as red squares, and fit as red dotted line); (b) isothermal M vs. H plots (squares) and corresponding fit (lines) for 1.85 (blue), 3 (green), 5 (yellow) and 8 K (red); (c) isothermal M vs. H/T plots (squares) and corresponding fit (lines) for 1.85 (blue), 3 (green), 5 (yellow) and 8 K (red).

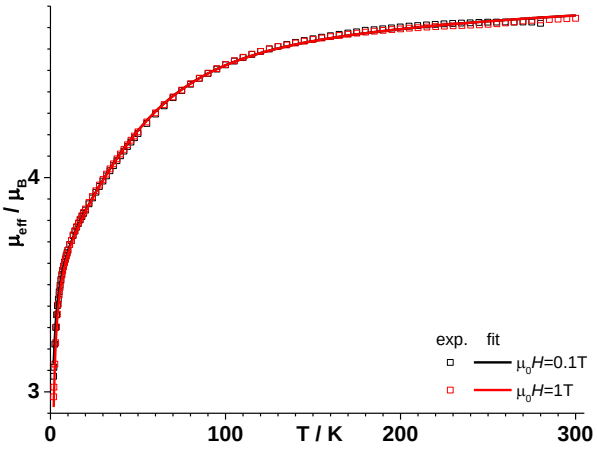

(a)

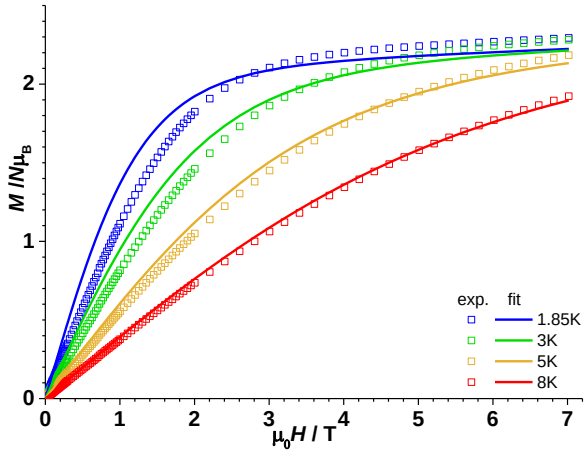

(b)

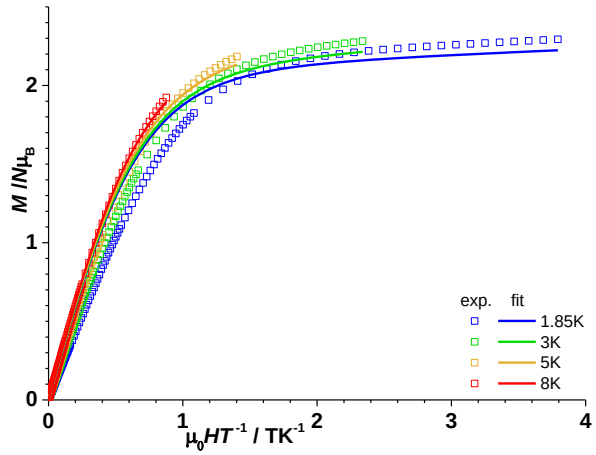

(c)

Figure S6. Magnetic behavior of $[Co(en)_3](NO_3)_2$. (a) μ_{eff} vs. T plot for magnetic fields of 0.1 (experimental points as black squares, and fit as black dotted line) and 1 T (experimental points as red squares, and fit as red dotted line); (b) isothermal M vs. H plot (squares) and corresponding fit (lines) for 1.85 (blue), 3 (green), 5 (yellow) and 8 K (red); (c) isothermal M vs. H/T plot (squares) and corresponding fit (lines) for 1.85 (blue), 3 (green), 5 (yellow) and 8 K (red).

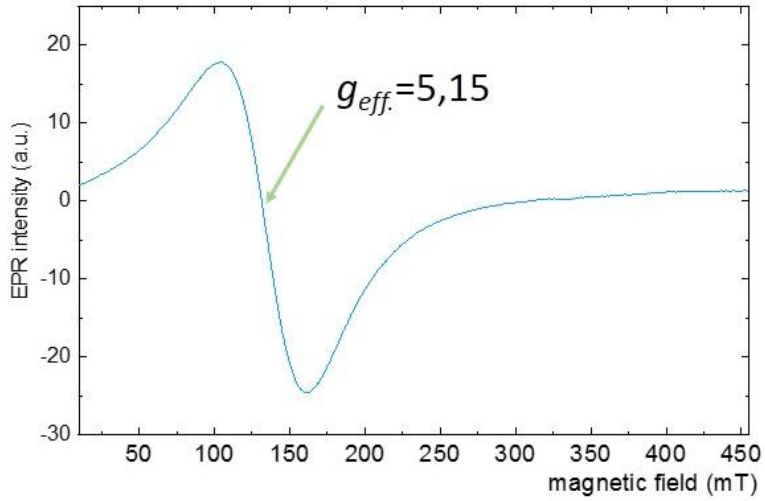

Figure S7. *X*-band (9.54 GHz) EPR of a polycrystalline sample of $[Co(en)_3](NO_3)_2$ at 5 K.

Protocol for Bragg peak examination:

A small piece (80 × 80 × 140 mm³) of a previously indexed crystal of [Λ-Mn(en)₃](NO₃)₂ was cut and mounted on a cryoloop using immersion oil. The crystal was put at 160 K on the Apex II goniometer. Cell parameters determination gave a = 9.073(10) Å, c = 11.131(17) Å, V = 793.6(17) Å³, with a mosaicity of 0.64°. Peaks were sharp, small and well defined. The goniometer positions to obtain [001], [101], and [011] in diffraction condition were calculated, and trial pictures were taken. Only the [011] pictures were satisfactory and a series of these were taken between 154 and 148 K every 0.2 K (4° w-scan, 300 s exposure time). The temperature was then decreased to 140 K, and the triple cell parameters were determined at that temperature: a = 9.042(8) Å, c = 33.29(3) Å, V = 2357(4) Å³, with a mosaicity of 0.63°.

As can be seen in Figure S8, rows of peaks along the c direction provide a direct indication of the occurrence of the transition and the tripling of the c parameter. The intensity of selected peaks, normalized against the 140 K value, is plotted in the Figure. As can be seen, Bragg peaks pertaining to the tripled unit cell begin to appear as high as 152 K in cooling mode, and the intensity of those satellite peaks is seen to increase down to 148 K, but with a further increase seen between that temperature and 140 K.

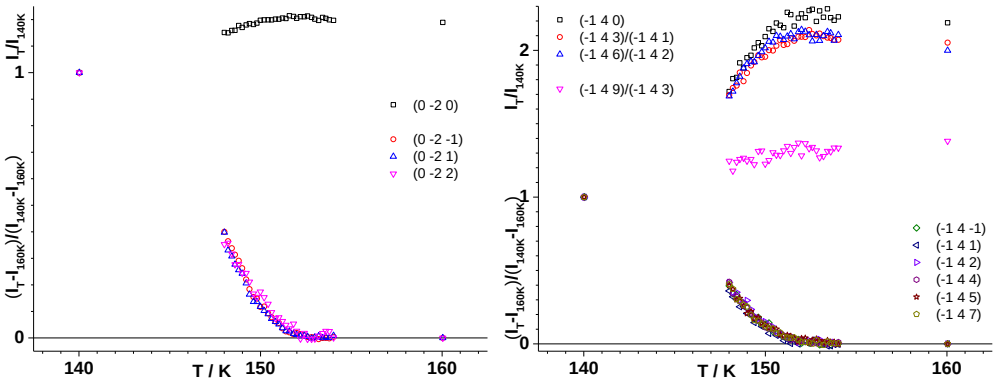

Figure S8. Variation of selected Bragg peaks with temperature.

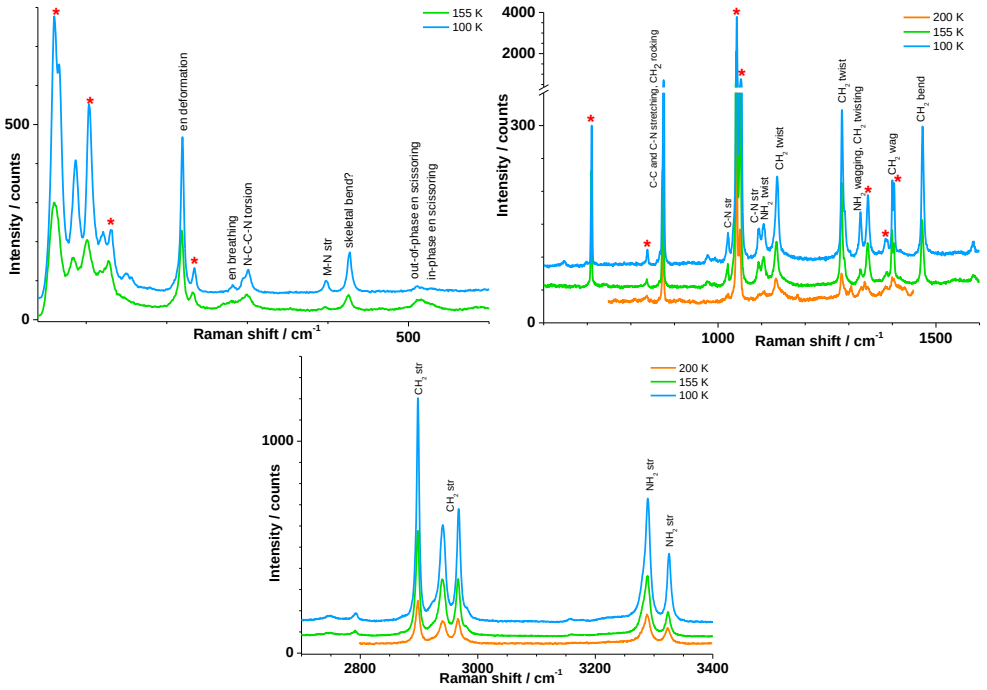

Figure S9. Variable temperature Raman spectra measured on a single crystal of $[Co(en)_3](NO_3)_2$ between 200 and 100 K in the low-energy range (top, left), the fingerprint range (top,right) and the C-H and N-H stretching range (bottom). Spectra are vertically shifted for clarity. Tentative assignments were made based on litterature data (see main text). Resonances attributed mainly to the nitrate anions are signalled with red stars.

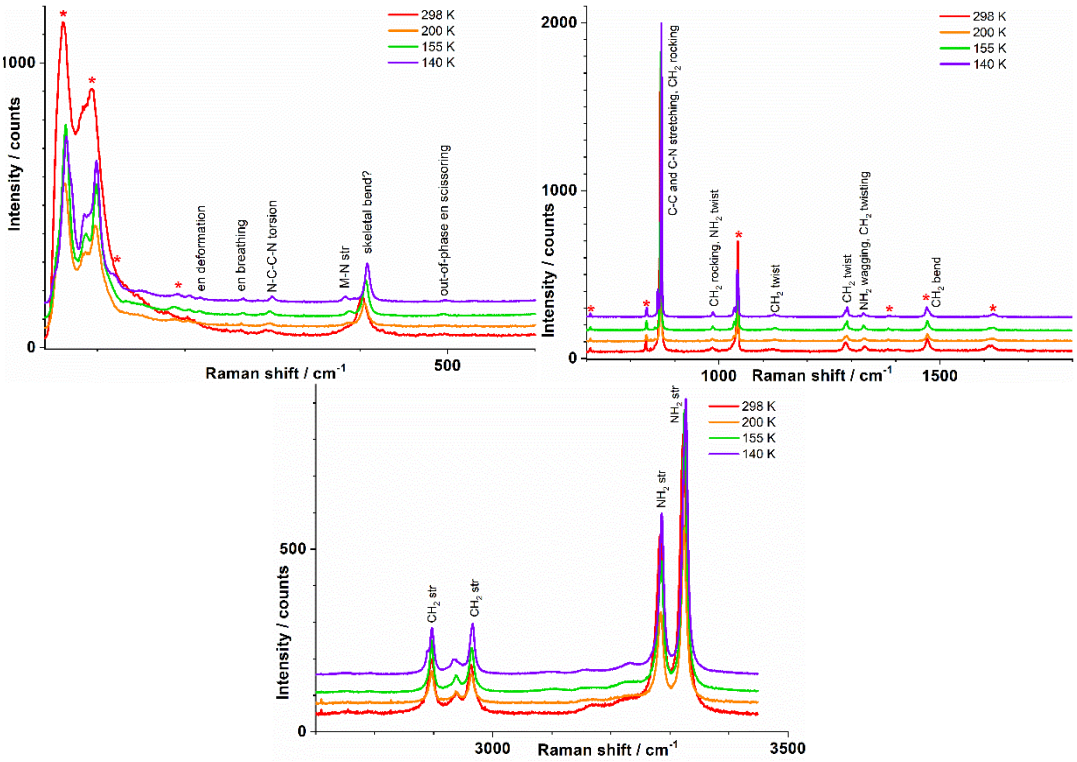

Figure S10. Variable temperature Raman spectra measured on a single crystal of $[Mn(en)_3](NO_3)_2$ between 298 and 140 K in the low-energy range (top, left), the fingerprint range (top, right) and the C-H&N-H stretching range (bottom). Spectra are vertically shifted for clarity. Tentative assignments were

made based on litterature data (see main text). Resonances attributed mainly to the nitrate anions are signalled with red stars.

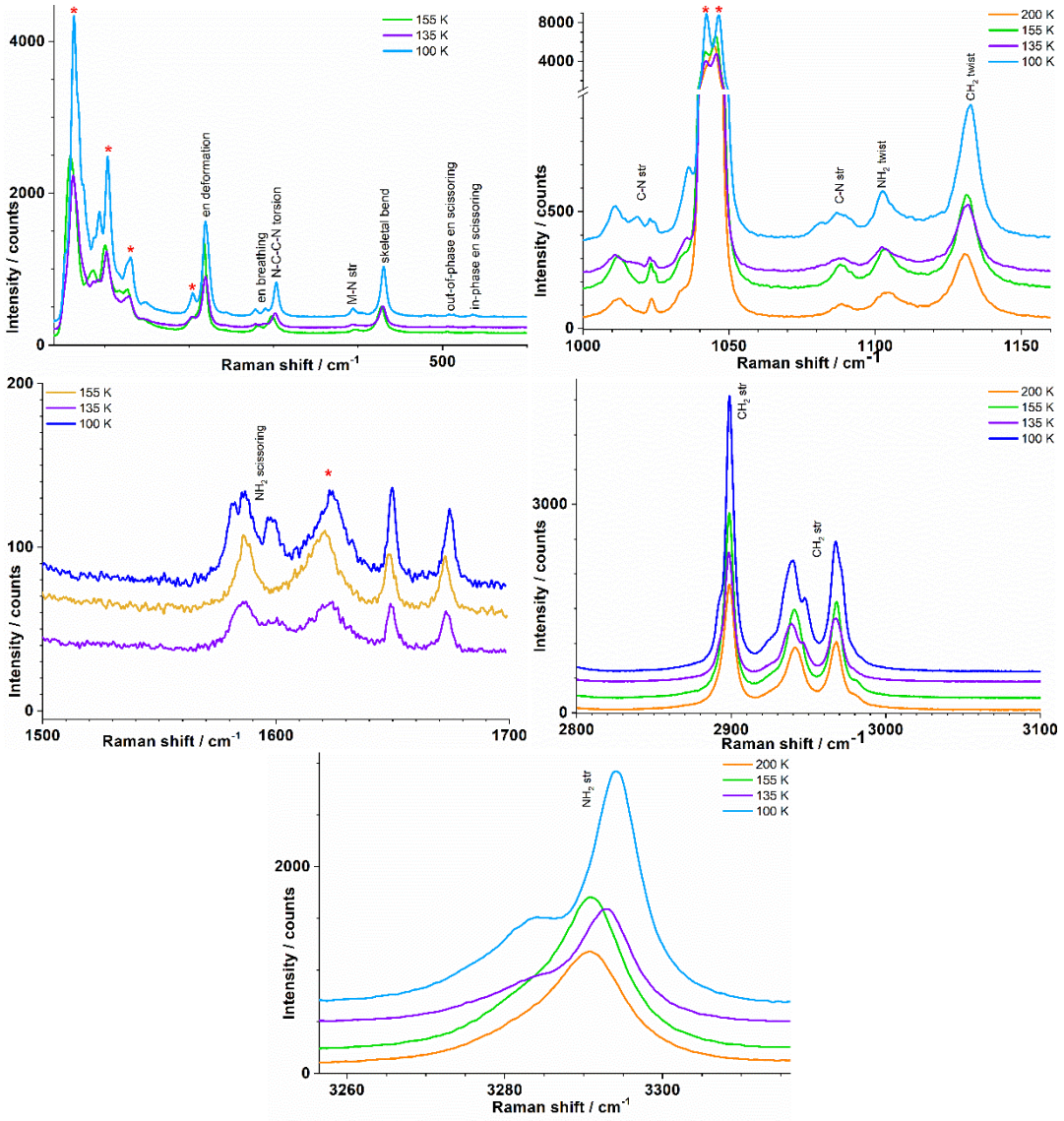

Figure S11. Variable temperature Raman spectra measured on a single crystal of $[Zn(en)_3](NO_3)_2$ between 200 and 100 K in the low-energy range (top), two zoomed regions in the fingerprint range (middle) and the C-H and N-H stretchings ranges (bottom). Spectra are vertically shifted for clarity. Tentative assignments were made based on litterature data (see main text). Resonances attributed mainly to the nitrate anions are signalled with red stars.

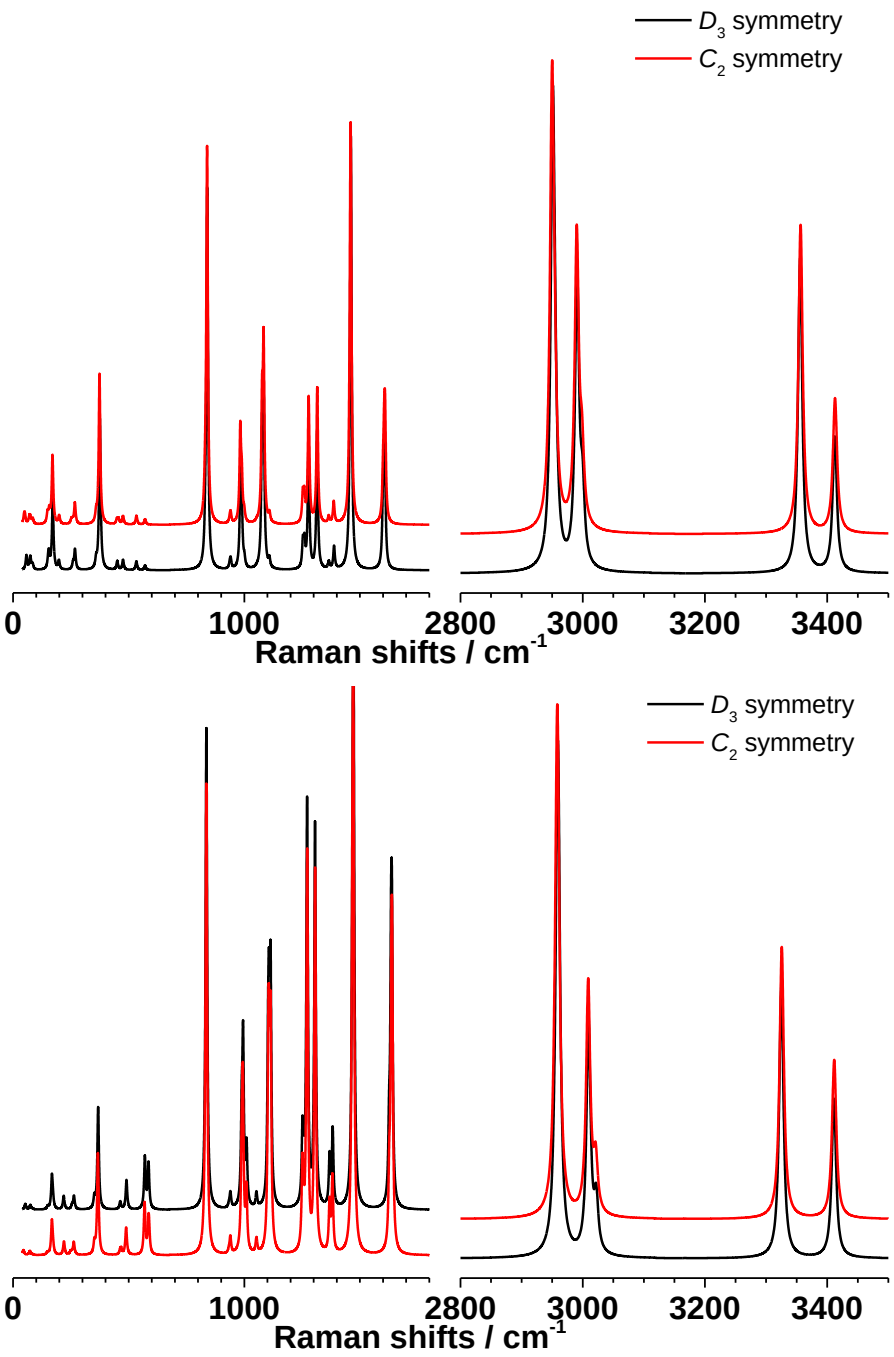

Figure S12. Comparison of Raman spectra calculated for $[Zn(en)_3]^{2+}$ from the optimized structures in D_3 (black line) and C_2 (red line) symmetries derived from the RAVJAZ and RAVJAZ01 crystal structures respectively, at B3LYP/cc-pTVZ (top) and B3LYP/LANL2DZ (bottom) levels. Spectra are vertically shifted for clarity.

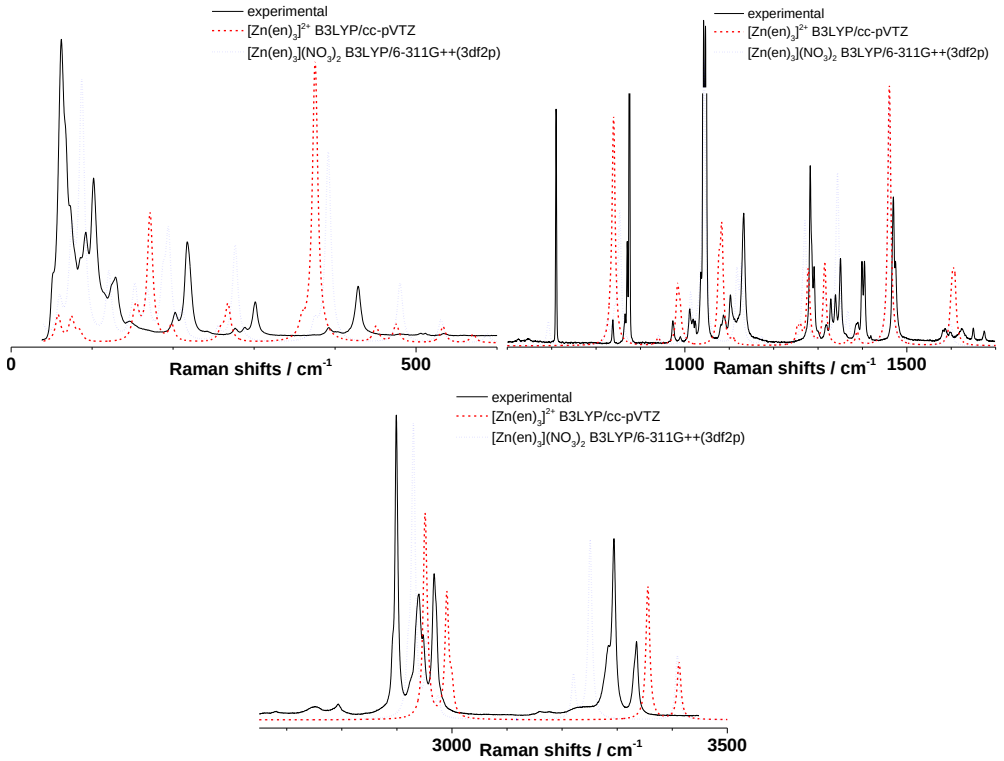

Figure S13. Comparison of Raman spectra measured at 100K (black line) and calculated for $[Zn(en)_3]^{2+}$ (red dashed line) and $[Zn(en)_3](NO3)_2$ (blue dashed line), derived from the RAVJAZ crystal structures, at B3LYP/cc-pTVZ and B3LYP/6-311G++(3df2p) levels respectively.